Configuration of the surface determination parameters for dimensional measurements with/using helpful metric as visualisation tool

Malik Enniafa, Valerie Kaftandjian, Anne-Françoise Obaton, Sébastien Brzuchacz

NDT net
e-Journal of Nondestructive Testing - ISSN 1435-4934 - www.ndt.net
13th Conference on Industrial Computed Tomography, Wels, Austria (iCT 2024), www.ict-conference.com/2024
eJNDT

Configuration of the surface determination parameters for dimensional measurements with/using helpful metric as visualisation tool

Malik ENNIAFA[1,2,3], Valerie KAFTANDJIAN[2], Anne-Françoise OBATON[3], Sébastien BRZUCHACZ[1]

[1]CETIM, 52 avenue Félix Louat, Senlis, France, e-mail: malik.enniafa@cetim.fr , sebastien.brzuchacz@cetim.fr

[2]Univ Lyon, INSA Lyon, LVA, EA677, 69621 Villeurbanne, France, e-mail: valerie.kaftandjian@insa-lyon.fr

[3]Laboratoire National de Métrologie et d'Essais (LNE), 75015 Paris, France, e-mail: anne-francoise.obaton@lne.fr

Abstract

X-ray computed tomography allows scanning the internal attenuation coefficient of a part. In X-ray domain, this coefficient highly depends on the materials. To perform a dimensional measurement from the volumetric data, a surface (i.e. point cloud) is required, on which a shape can be fitted, and measurements of volumes or surfaces, and even rugosity can be evaluated. To extract this point cloud from the volume, different configurable algorithms exist, using different criteria. This can have an impact on the extracted surface and thus on the dimensional measurement and its uncertainty. A parametric study of the influencing parameters of the XCT measuring chain has been performed, using CIVA RT/CT software to model the tomographic acquisition and Python programs to extract the surface. This allows to have a better understanding of the sensitivity of the influencing parameters in the dimensional uncertainty, and to make some recommendations for the surface determination.

Keywords: X-ray Computed Tomography, dimensional measurement, surface determination, acquisition parameters, visual metrics, artefacts

1 Introduction

X-ray Computed Tomography (XCT) is a non-destructive technique which provides a 3D representation of the volume, more precisely its attenuation coefficient which depends on the material. The tomograph provides projections (digital radiographs) to the algorithm which reconstructs the volume. Inside this volume, the value of the attenuation coefficient varies from low value for the air to different higher values for the part's materials. In addition to defect analysis, dimensional measurements can be performed from that volume. To do so, a surface between the values from air to the part's material needs to be defined. Dimensional measurements are performed from that surface like would be done commonly using optical coordinate measuring machines. However, the complex measuring chain of XCT for dimensional measurement involves influencing factors that lead to deviation from the true value of the measurand. For instance, these factors can be the acquisition parameters [1–5]. Due to some inexact reconstruction algorithms (FDK based [6], used for its speed), the shape and materials of the part or its orientation in relation to X-ray trajectories [7–9] can also cause deviations. This is very problematic when providing an uncertainty on the measurement. The most commonly used uncertainty estimation method is based on the substitution method [10]. However, the fact that in XCT the bias is highly dependent of the scanning parameters, of the measurand and of the part (geometry and material) [11, 12], gives incompatible or overestimated uncertainties while estimated with this method [12]. Furthermore, it had been shown that some surface determinations are more repeatable than others (see work in [13–15], and respectively description of gradient and grey value-based surface determination in [15]). In this paper, an investigation of the parameters used for surface determination as well as the criterion used for the surface positioning in the volume (usually threshold for grey value approach, or when the gradient is maximized, i.e. a derivative approach) are presented. Different magnitude of XCT artefacts with different surface determination setups have been investigated in order to understand their impact on the dimensional measurement. The scans are acquired through simulation software CIVA, which also provides the reconstruction algorithm (FDK). The custom surface determination algorithms are implemented in Python; thus their operating is entirely known. The dimensional measurements are carried out with PolyWorks.

2 Material and Method

2.1 Part description

A reference part for the substitution method is investigated and used in this study. The mono-material part is made of aluminum. The part and the denomination of the selected measurands are displayed in figure 1. The part is very complex on purpose, to assess the influence of the parameters of the pipeline for different sizes, different positions and orientations of the measurands, as well as different penetration paths (total length, varying lengths). All the shapes are empty of matter. Its externaldiameter is 100mm, the maximal ratio of thickness variation ($\frac{maximum}{minimum}$) is $\frac{100}{10} = 10$

https://doi.org/10.58286/29281

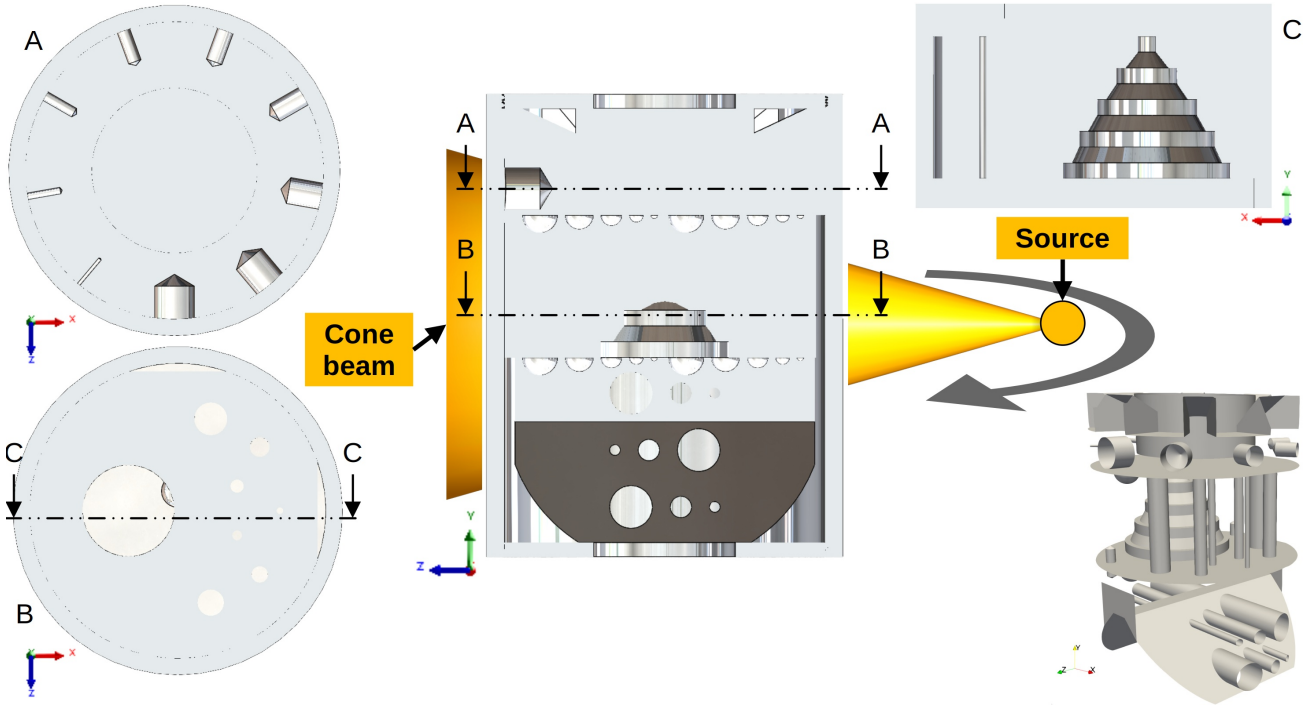

Figure 1: XCT phantom with multiple shapes (cylinders, cones and spheres of radius from 1mm to 12mm), and several positions (height and radial) and orientations (vertical or horizontal).

2.2 Simulated acquisition setups

In this study, XCT scans are obtained with the simulation software CIVA RT/CT enabling to simulate different acquisition parameters and characteristics: different source energy spectra, physical filtering of the output X-ray, noises, blurring or even physical phenomena like X-ray scattering. Indeed, CIVA RT/CT can simulate scatter effect through a Monte Carlo simulation, even with a monochromatic spectrum (which remove artefacts due to the filtering of X-rays by matter). This allows to investigate the consequence of XCT artefacts on dimensional measurements individually, which is not feasible in practice as some deviations are also caused by temperature, and misaligned axis. Furthermore, the ideal scan configuration (monochromatic spectrum, free from any noise), which is not physically possible, serves as a baseline. In these conditions, one can have a better understanding of the impact of artefacts on dimensional measurements.

Five Scan are investigated, classified from the closer modeling to the reconstruction's hypothesis to the most away one 1.

Table 1: Scans description.

Scan name	Scan description	Source	Detector
MonoAnatq	Also referred as Ideal scan since there is no XCT artefacts except cone beam circular trajectory and sampling artefacts.	Monochromatic 100 keV, punctual source, no filter	no noise, no blurring
MonoMC100	Realistic monochromatic scan, with XCT artefacts except beam hardening ones.	Monochromatic 100 keV, 1 vx[1] spot size, no filter	complete noise, gaussian blurring MTF[2] 20% at $33cm^{-1}$
PolyMC1Sn	Realistic polychromatic scan for heavily filtered source, with all XCT artefacts but in an "acceptable" quantity.	Polychromatic 225 kV, 1 vx spot size, 1mm Sn filter	complete noise, gaussian blurring MTF 20% at $33cm^{-1}$
PolyMC1Cu	Realistic polychromatic scan for moderately filtered source, with all XCT artefacts, still in an "acceptable" quantity.	Polychromatic 225 kV, 1 vx spot size, 1mm Cu filter	complete noise, gaussian blurring MTF 20% at $33cm^{-1}$
PolyMC0mm	Realistic polychromatic scan for unfiltered source, with all XCT artefacts, but too strong for a realistic use case (also referred as *worst scan*).	Polychromatic 225 kV, 1 vx spot size, no filter	complete noise, gaussian blurring MTF 20% at $33cm^{-1}$

[1] Voxel abbreviation, the voxel size used in this paper are of 150µm.
[2] Modulation Transfer Function.

The magnification is $m = \frac{800}{600} = 1.33$, no axes default are introduced. The detector is always the same: a CsI 200µm thick scintillator with 1024 × 768 200µm spaced pixels. The reconstructed voxel size is 150µm. The number of projections is the same as the detector width: 768. As shown in [2], a number of projections close to the width of detector is enough for size measurements. The polychromatic configurations uses different physical filter (Sn, Cu) or none. The worst scan (PolyMC0mm) is a realistic simulation, but present too much artefacts to be used for a realist use case (except for research matter). No XCT artefact corrections were applied. The exposure time is adjusted such as to reach 63000 grey values on the detector without the part in the field of view.

2.3 Principle of surface determination

2.3.1 General steps

In XCT, the surface determination can be seen as a 3-steps algorithm:

1. Labeling the voxels of the part. This is called segmentation. This step does not output a surface (segmented voxels are still volumetric data) and its resolution is the voxel's size.
2. Generating a point cloud between the part's voxel and the non-part's voxels. The output is now a surface, but the resolution is still the voxel's size.
3. Adjusting the position of each point based on the neighbor grey values and a criterion defining the surface. The output is a surface with a subvoxelic resolution.

This study covers the last step where the position of the surface (point cloud), with a subvoxelic resolution, is truly decided. Historically, the surface determination was done with the Marching Cubes algorithm [16], in which the adjustment of points was made using linear interpolation between two voxels. The orientation along which the voxel position is adjusted can only be one of the three axes of the voxel grid. With much more computing power nowadays, it is possible to consider a better orientation, normal to the border of the part in XCT volume. Furthermore, it is possible to consider a longer range than 1vx, as several commercial software do. However, the precise location of the part surface in the XCT data should be defined, using either a global criterion or a local one.

2.3.2 Criterion to define the surface in the XCT volume

The definition of the surface is based on an underlying criterion, which can be of 2 natures: a chosen grey value (global, i.e. for all the points) or a characteristic on the local gradient (per point). For each criterion, the surface determination algorithm consists of extracting the surface at the matching position of the criterion. In our work, we distinguish between the definition of the surface (based on a criterion) and the way of extracting the corresponding surface (the algorithms and implementations) because each criterion leads to different implementation algorithms (see figure 2). It is not fair to compare different algorithms if they are not based on the same criterion, this is why the distinction is important.

By introducing this "new" vocabulary (criterion for XCT surface adjustment), we make obvious the influence of the implementation (aside from surface criterion) on the dimensional errors. In our implementations, all criteria share step A and B, which reduces further the bias of the implementations. The influence of the criterion choice will be investigated for different level of XCT artefacts to allow a comparison in any situation.

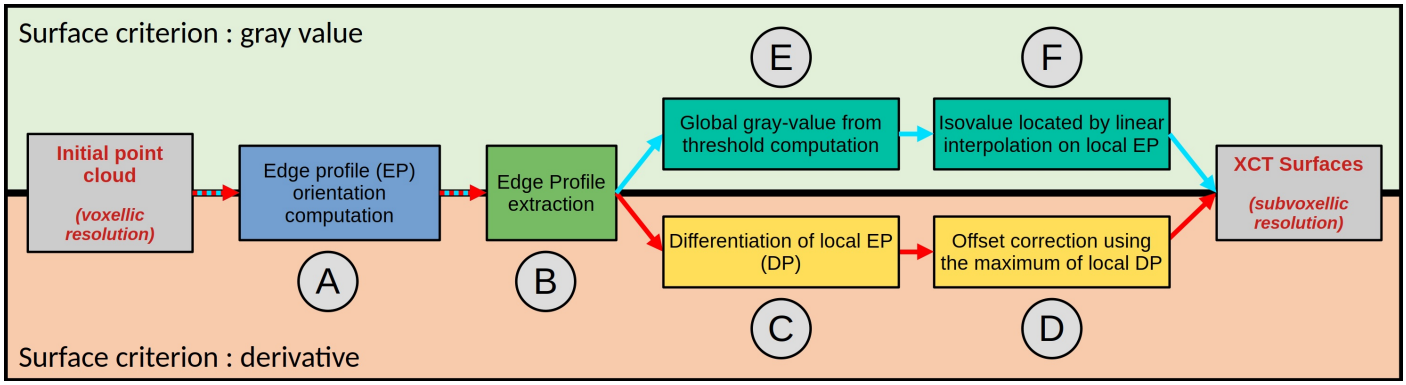

Figure 2: Steps of the two pipelines for the respective surface determination criteria and associated algorithms.

The situation is analogue for the fit algorithms, used in dimensional metrology, giving the characteristics of a shape (radius of a sphere, orientation of a plane, etc.). The fit algorithm will try to fit a shape through a point cloud, based on a chosen criterion. This criterion could be "minimizing the sum of squared distances of residuals", or "the maximal inscribed diameter" for example. Choosing different criteria will certainly leads to different shape characteristics, as it is seeking something (a definition) different. Different algorithms based on the same criterion should converge more or less well to the same characteristics (as they try to solve the same – minimization – problem). This is the same for the surface determination algorithms.

For the gray value-based criteria the global histogram of XCT values is computed. Three different thresholds are considered (see figure **??**:

1. the middle distance between the maximums of each population (air and part)
2. the middle distance between the geometric centers of the area of each population

3. the Otsu threshold (minimization of the intra-variance or maximization of inter variance).

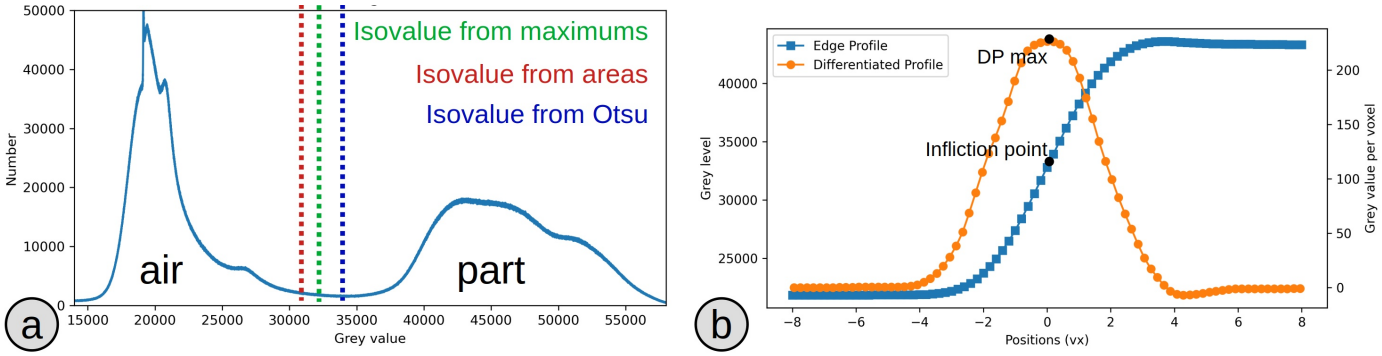

Figure 3: Different criteria: a) gray value-based (in this work, based on histogram computations) and b) gradient-based (in this work, the maximum of the derivative of edge profile).

For the gradient (derivative) criterion, the grey value profile along the border (edge profile in blue in figure 3b) is extracted. A normal edge profile shows a change in convexness, which occurs at the "infliction point". At this point, the first derivative is maximum. The gradient criterion is based on the definition of the surface at this infliction point, corresponding to the maximum of the first derivative profile.

2.4 Implemented algorithms of surface extraction

Once the point cloud is obtained after general steps 1 and 2, the adjustment of the surface begins. The starting point consists in extracting the edge profile (see figure 2AB). Indeed, extracting the local edge profile is a shared step for both algorithms, because the point adjustment will be done along this line.

2.4.1 Edge profile extraction

It can be seen as a 2 steps process: obtaining the normal vector to the border and extracting the grey values along this orientation. This is important as the contrast is maximum along this direction as illustrated in figure 5 (green line). If the orientation is searched only along the three principal directions of the volume, as done by the Marching Cubes algorithm (one of its drawbacks), the edge profile can be spread out (see red line in figure 5). For this reason, it is called here "voxel grid" approach, and is used for comparison.

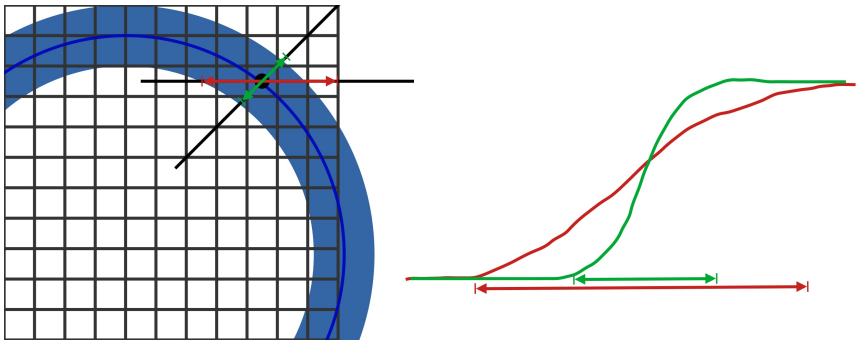

Figure 4: Difference in edge profiles for an orientation following only the voxel grid's orientation (red) and another which seems more normal t the part's border (green).

A way to compute a better orientation for the edge profile in the volume is by computing the 3D gradient orientation (using 3D Sobel filter) – here named "gradient". In figure 5a, the "gradient" orientation seems better (more contrasted) than the "voxel grid" orientation because of the thickness of gray value transition from air to material (see figure 5).

In real scans, noise, coupled with XCT artefacts and blurs, can influence the computation of the edge normal orientation. To address the influence of noise, smoothing the volume before the gradient computation is proposed. Note however that this pre-smoothing is only aimed to improve the computation of orientation but the extracted edge profile is not smoothed. An example is shown in figure 5a: the orientation obtained with the gradient method is nearly normal to the border, and is better with a pre-smoothing. The spread out of the edge profile is clearly visible with voxel grid method.

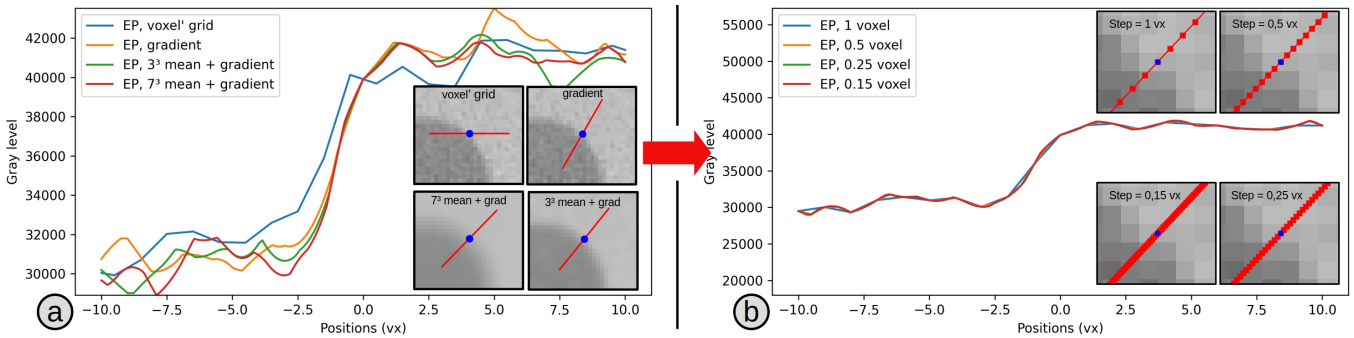

Figure 5: XCT volume's edge profile extraction.

Once the orientation is found, the edge profile can be sampled at different resolutions (see figures 5b). First of all, the coordinate of the sampled points of edge profile are determined, then their grey values are obtained thanks to trilinear interpolation (bilinear if the orientation has two components and linear if it has one). Note that the profile is centered around the "0" (the origin), which is the initial position of the surface, but does not necessarily correspond to the infliction point of the profile nor the grey value criterion. The origin is the center of the red line in figure 5, positives values of the EP position index represent part grey values and negatives represent the air. Surface determination algorithms consist of searching the offset between the initial surface point position (origin) and the position matching the chosen criterion. As all the criteria are sought on the edge profile, an offset from their position to the point (origin) is computed, and then it is applied along the computed orientation (normal to the border). The surface is adjusted along these normals. Thus, a small sampling step of the edge profile gives a better sub-voxellic resolution in the final surface adjustment.

2.4.2 Implementation for grey value criterion

For the gray value-based criterion, the matching isovalue position on the edge profile is found using linear interpolation (see figure 2F). If several isovalues are found in the edge profile, the closest from the origin is used.

2.4.3 Implementation for maximal gradient criterion

The different steps for surface determination, implemented in the presented algorithm for the derivative criterion, are presented in figure 2ABCD. To find the infliction point, the edge profile is firstly differentiated with a 1D derivative filter (Prewitt). The result is called DP (Derivative Profile). The size of the filter can vary, the larger its size, the more spread out the DP (see figure 6). As a first approach, the position of the maximum can be the highest point of the sampled DP. The distance between the origin and the DP highest point is called offset. The surface point is adjusted by this offset along the computed orientation (see the red line figure 5). This limits the resolution of the offset value to the edge profile sampling step.

In figure 6 (filter of size 3), several maximums have been identified: the highest one is chosen. Noise and artefacts impact the seeking of the DP maximum. They can cause a bias on the maximum DP position and the apparition of secondary maxima. In practice the derivative filter size becomes an influent parameter. In the end, the implementation of the derivative criterion contains the following parameters:

1. the orientation method: voxel / gradient / pre-smoothed gradient (with a varying filter size from 3^3 to 11^3)
2. the EP sampling step (from 0.05vx to 1vx)
3. the derivative filter size (from 2vx to 8vx, i.e. the number of points depends on the sampling step)

As mentioned in the literature [13–15], the first derivative criterion seems always better. Consequently, in this parametric study of the algorithm's parameters (implementation), the derivative criterion is considered.

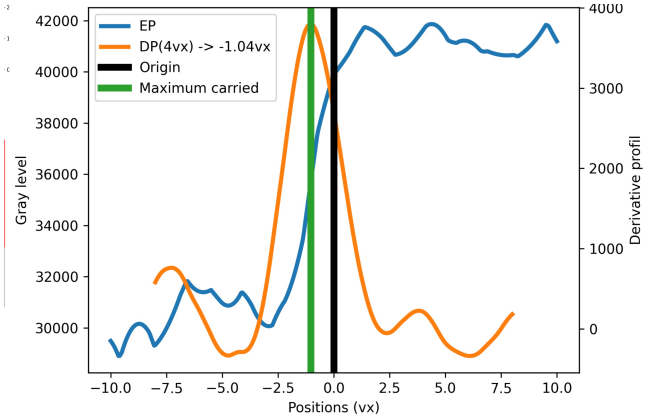

Figure 6: Main steps of the implemented algorithm for surface determination with derivative criterion.

2.5 Measurands and their references values

In this study, measurands are extracted from 51 shapes (cylinders and spheres) using least square fits. For one shape, two measurands are estimated:

1. The error on diameter, which is the reference value minus the XCT value: Derror = Dref DXCT
2. The standard deviation of residuals (the residual is the distance between a XCT surface point and the fitted surface, illustrated in figure 9d). It is used to describe the noise level of the surface point of a measurand.

For sake of simplification, only the average values as well as their standard deviations across all shapes are shown. Of course, for the average error on diameter, the absolute values of errors are considered (the vast majority, but not all, are negative).

The question of the reference for the measurands is an important matter when using simulation software as it can introduce a bias despite the well-controlled acquisition. The CAD file formats uses NURBES to manipulate continuous shape. When designing the part, the user set its nominal characteristics, such as the diameter of a cylinder. This step is illustrated at figure 7a.

Unfortunately, XCT simulation software needs a discrete file format such as "STL" (triangulated surface and their points). The meshing algorithms have parameters and presets to produce different levels of meshing resolution. The STL file created from the CAD had all its points correctly located on the CAD surface (see figure 7b). Using a dimensional analysis software (or a fitting function on points) to obtain the surface of the STL will give the same value as the CAD design, despite the STL' faces not coinciding with it.

When simulating the XCT acquisition, the simulation software uses rays that go through the part (see figure 7c). The average length of the rays is smaller than it should be due to the STL discretization of the CAD surface. It is here a 14.996mm diameter.

In figure 7d, the XCT volume is reconstructed from projections, and the surface extracted. The fitted diameter is different from the CAD because the probed penetration length during simulation was smaller (STL error), but it is also slightly different from the average penetrated length during simulation. This is because of the inexact FDK, sampling irregularities and interpolations that occurs (FDK and surface determination).

The correct way to obtain the STL diameter, is to sample the generated STL surface with points, and use them for the fitting (see figure 7e). This is done with the software VG Studio in this work.

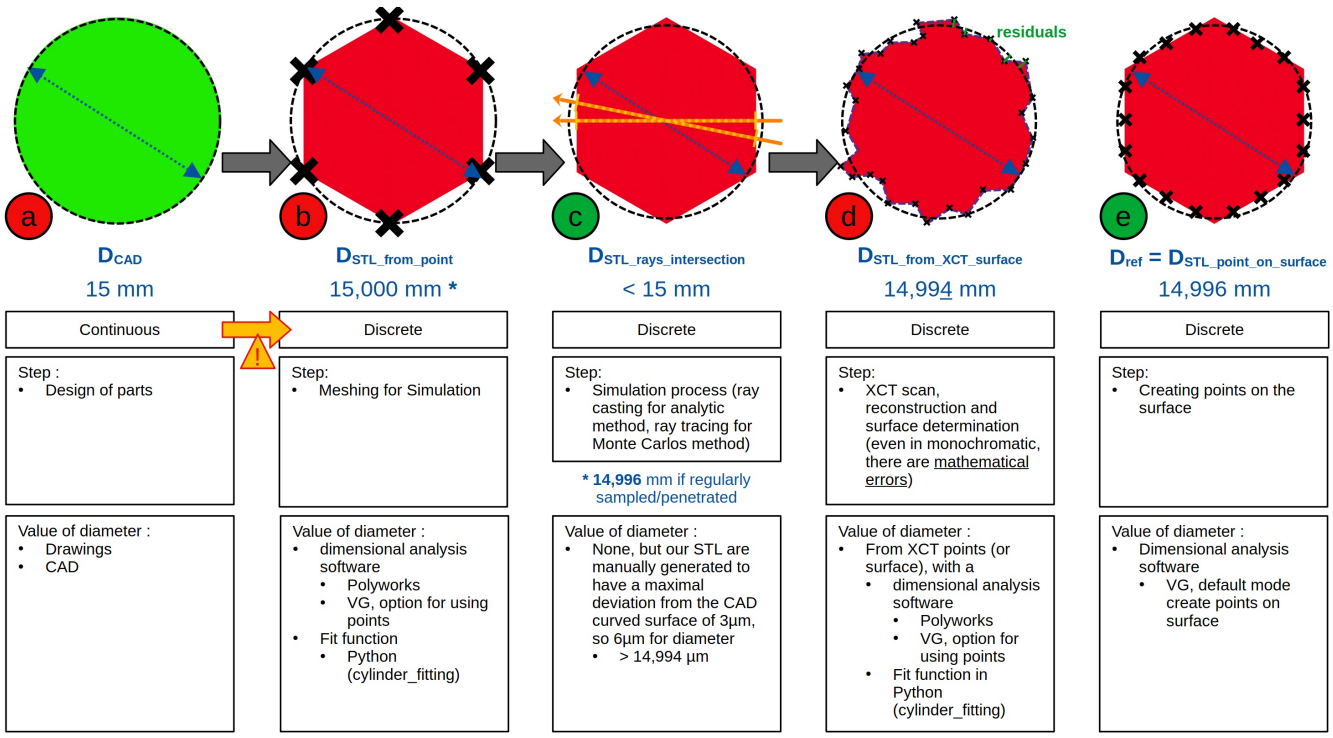

Figure 7: Possible reference values during the XCT measure process for simulation, and the right way to obtain it (last on right).

3 Results

The different simulated scans, presented in table 1, correspond to different levels of artefacts, from the lowest level (MonoAnatq, see table 1) to the worst (PolyMC0mm, see table 1). Of course, the highest level of artefacts will never be used in a real configuration, but it is useful here for comparison. The results will be presented using the metrics described earlier (see 2.5).

3.1 Criterion study

It is important to mention that the edge profile extraction is a shared step of implementation for both criteria which allows to compare them in a fair way (see figure 2). For all the following results the orientation is computed by the pre-smoothed gradient filter (size 3^3) and the EP sampling step of 0.05vx. In figure 8a, the average of absolute diameter errors is shown for each scan for the grey value criteria using the three thresholds and compared with the derivative criteria.

A first observation is that the ideal scan still presents an error which is less important for the derivative criterion. This means that, even when no physical effect degrades the scan, some error still exists which are due to partial volume effects and reconstruction algorithm. The averages of errors increase with the level of XCT artefact, which is the expected behavior. Indeed, a more filtered source tends to reduce the average errors. However, it should be noted that the noise level is the same for all scans, because the integration time is adapted to have the same signal when there is no part attenuation. In a realistic use case, the operator has a limit of time, so the filtered scans will probably have a lower signal to noise ratio. The heavily filtered scan configuration is close to the monochromatic one with noise and scatter. The biggest difference between the scans lies between the ideal scan and the latter one, which indicates the importance of noise. Another very big difference is observed for the unfiltered scan, which gives, of course the highest errors.

For every scan configuration the derivative criterion gives always a much less average error. For the grey value-based criterion the errors lie around 1vx for the best realistic scans (MonoMC100/ blue and PolyMC1Sn/yellow), and the influence of the thresholds is negligible. For the two worse scans the errors are much higher and vary much more with the threshold. Due to the XCT artefacts varying in the volume, the grey values of air and material can be biased, and so a bias in the surface positioning can be created locally. The derivative criterion has no such issue, as everything is only computed with neighboring voxels, and the errors are much lower (less than one third of a voxel even for the worst scan). The evolution of average error between the configurations (from the less "artifacted" to the most), is slower for the derivative criterion than for the grey value one. This indicates a higher sensitivity of the grey value criterion to XCT artefacts (in presence of noise).

Then the standard deviation of errors is shown in figure 8b. A high value indicates a high dispersion of errors between the different measurands, which is mostly due to the part geometry in the volume and the energies used (X-ray spectrum). Thus, it indicates the sensitivity of the dimensional measuring chain to the presence of XCT artefacts, which is an indicator of robustness towards XCT artefacts.

The standard deviation increases with the level of XCT artefacts. Contrary to the average errors, the evolution between the Sn filtered scan to the Cu, is much bigger. It is also bigger between the Cu filtered scan and unfiltered one. It means that with the Cu filtered scan some measurands are very far from the average even if they do not influence so much the average.

The derivative criterion is again the best. It has a lower standard deviation, with a slower evolution between the filtered scans, so it seems less sensitive to XCT artefacts. The derivative criterion highly limits the degradation of errors for measurands that seems to have "an acceptable level of XCT artefact", even for the unfiltered scan configuration.

The derivative criterion is the best because the errors are a lot smaller than the gray value criteria. The standard deviation is also reduced, and this confirms the previous observations where a derivative criterion was found more repeatable than a grey value one [13–15]. The derivative criterion is in fact less sensitive to XCT artefacts due to the fact that the computation for adjustment of the surface is done locally.

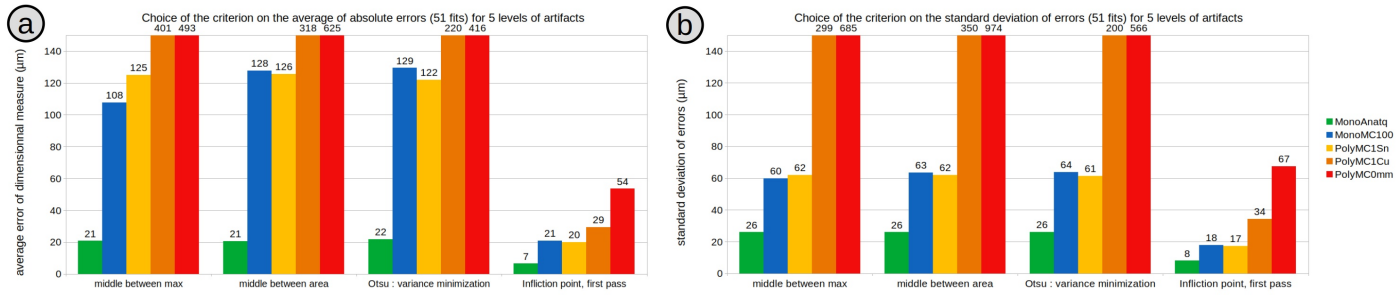

Figure 8: Influence of the criterion for surface determination and related parameters on a)the average of absolute errors, and b)the standard deviation of errors, for the different scans. Note that the scale is truncated to 150µm for better visualization.

3.2 Parametric study for the derivative criterion implementation

In this section, the objective is to illustrate the influence of the choice of the different parameters in the implemented pipeline for the derivative criterion only.

3.2.1 Edge profile orientation computation

This step is illustrated in figure 5a. Figure 9a shows the average of absolute diameter errors per scan for different orientation computation methods. As a general observation, the influence of the orientation computation is not very high, especially for the

ideal scan and the filtered ones. However, for the unfiltered scan, the influence is much more visible and the pre-smoothed gradient orientation with a size of 3^3 is the best.

The same can be observed also on the standard deviation of errors (see figure 9b). However, the standard deviation for the voxel grid is much higher for all scans which indicates a higher sensitivity to artefacts. This higher sensitivity for the voxel grid method is also visible on standard deviation of residuals (see figure 9c). This is also illustrated in figure 9d, where the point cloud after adjustment is shown for an example of cylinder. It can be seen that the surface of the cylinder is more "noisy" when the EP is plotted along the voxel grid orientation, whereas the gradient method using an EP along the true normal orientation is much better. Furthermore, the surface using the derivative criterion is noisier along the Y (vertical) orientation. The best choice results of a compromise: it seems to be the gradient with minimal pre-smoothing, because it is always close to the best choice in each graphs. For the following results, the default parameter value is the pre-smoothed gradient with a 3^3 filter size.

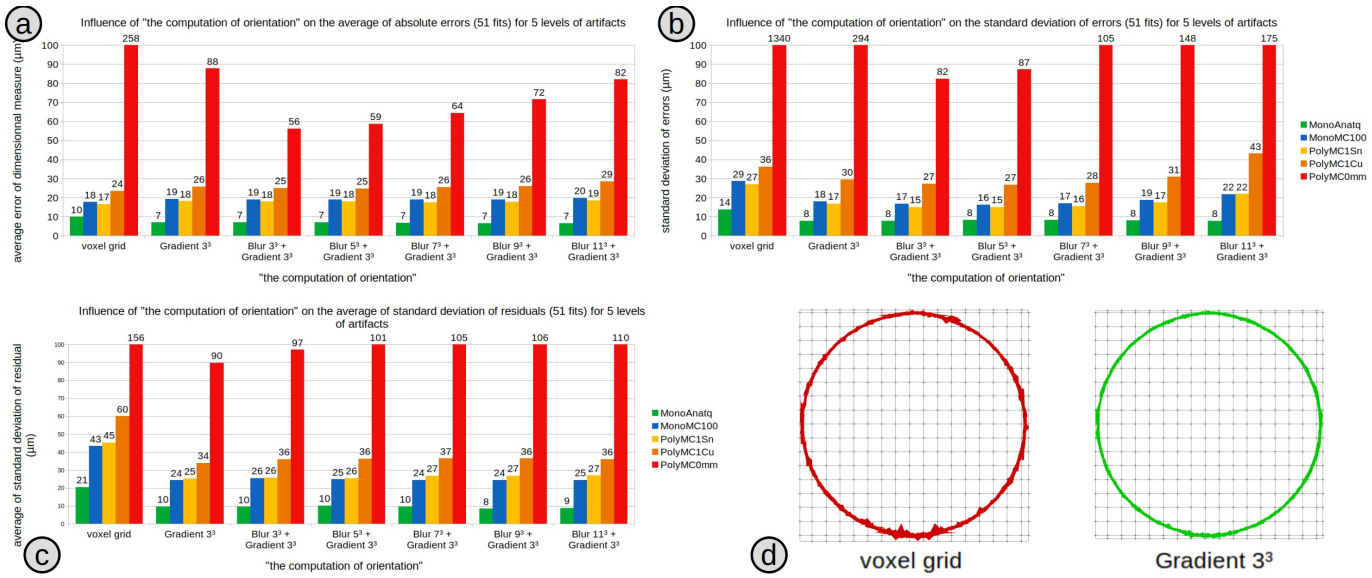

Figure 9: Influence of the orientation computation on a) the average errors b) standard deviation of errors and c) the average of standard deviation of residuals per scan d) representation of the adjusted points for a cylinder when the orientation is computed along the voxel grid (red) or along the true normal (green).

3.2.2 Edge profile sampling

This step is illustrated in figure 5b. The better the edge profile resolution, the better the resolution used for the offset computation, and thus, the better the final resolution of the surface adjustment. However, the influence of this sampling step in the average error is not so important, especially below 0.15 voxel, as visible in fig 10a. The reason is that the interpolation grid (represented in green in figure 10b) is fixed, and when the edge profile crosses the interpolation grid, not all the new points intersect the interpolation grid. In other words, there is an improvement in the offset computation only if new sampling points appear when the edge profile is better sampled (orange points in figure 10b). Figure 10c shows the corresponding edge profiles. For the following results, the default value is 0.05 vx in order to get the best spatial resolution in the offset computation.

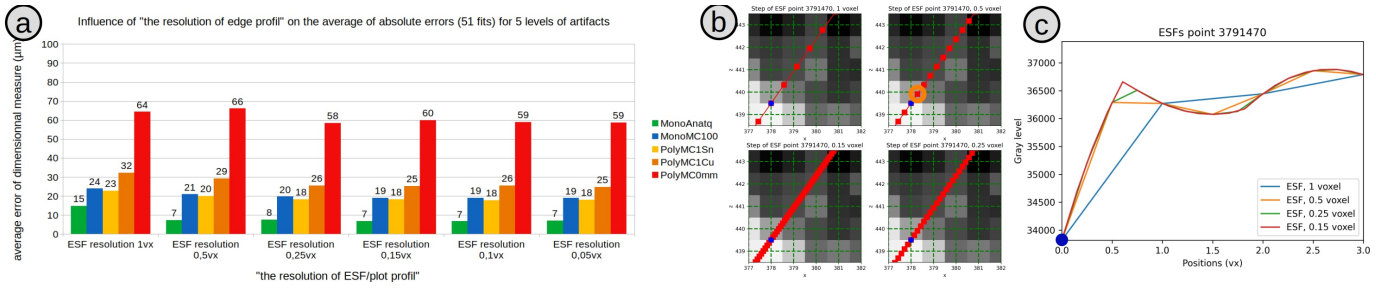

Figure 10: a) influence of the EP sampling step on the average absolute error, b) zoomed image of a border, where the interpolation grid is illustrated in green, and EP with different sampling steps (red points), where the orange point is an example of point crossing the interpolation grid; c) example of EP with different sampling steps.

3.2.3 Derivative filter size

The derivative filter size step is illustrated in figure 6. Figure 11a shows the average of absolute diameter errors per scan for different sizes of the derivative filter. The variations of these average errors differ depending on the type of scan. For realistic scans (blue, orange, red, i.e. noisy monochromatic et filtered polychromatic scans) the smallest derivative filter size is better because it allows to catch more precisely the maximal slope of the edge profile. Indeed, if the filter size is too high, the differentiation concerns not only the slope part of the edge profile, but also its borders. However, for the non filtered scan, there is an optimal size because increasing the filter size allows to decrease the sensitivity to noise. Going from 3vx to 4vx size, a drop by 70% of the average error is observed. A smaller filter size will provide a more symmetrical DP, but also new maxima due to an increasing sensitivity to noise.

Concerning the standard deviation of errors (fig 11b), a higher filter size tends to decrease the standard deviation because the influence of the position of the different measurands is less important with a big kernel window. For all scans, increasing the filter size decreases the standard deviation of the standard deviation of residuals. Nevertheless, beyond 4vx, the benefit of a long filter is less significant. For realistic scans, the choice of the derivative filter size results from a compromise. A small filter size is better to reduce the average errors but causes over voxel errors due to a greater sensitivity to noise. The right choice seems to depend on the nature and amplitude of the noise and artefacts.

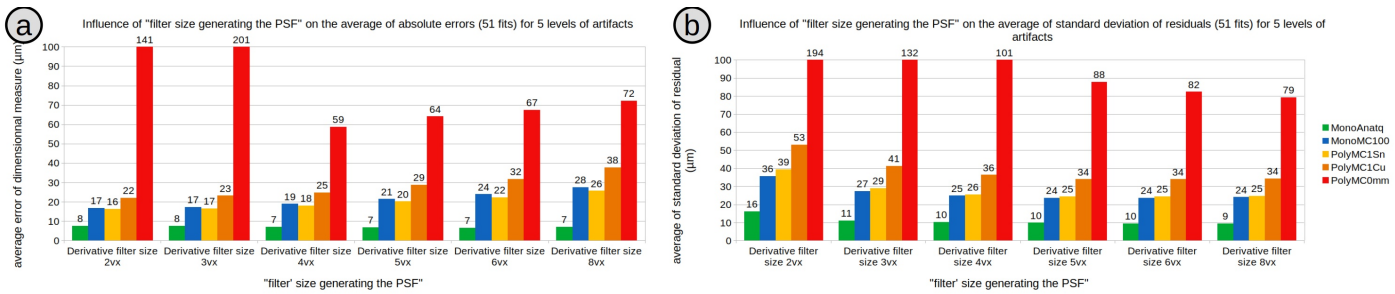

Figure 11: Influence of derivative filter size on a) the average of absolute errors and b) the average of standard deviation of residuals.

3.3 Visualization of influent factors

The previous results have shown that implementation parameters have an influence more or less important on the average errors. Moreover, the standard deviations of errors, but also the standard deviation of residuals also vary. As the reference part has been designed to contain a high variety of measurands, with very different location in the cone beam, it is interesting to help the operator with a visualization tool.

The following figures show the local slopes of the edge profile (figure 12a), as well as the FWHM of the derivative profile (figure 12b) which are two correlated parameters. The worst scan has been selected for illustration, in order to enhance the visualization. A high slope (resp. a small FWHM, for an excepted gaussian DP) indicates a higher local gradient, which can be highly modified in the presence of artefacts.

Using such a tool, the operator can choose the XCT acquisition parameters in such a way to prevent artefacts in the region of interest of the measurands.

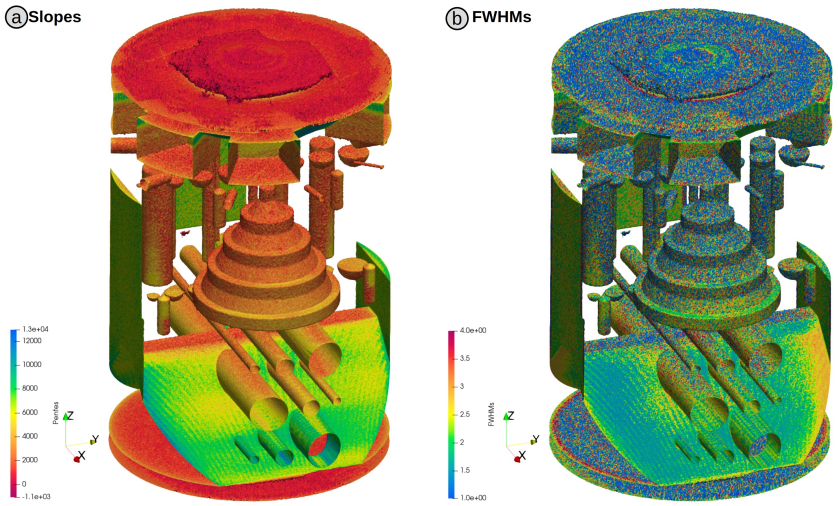

Figure 12: XCT extracted surface textured by a) slopes and b) FWHMs computed on each points.

3.4 Conclusion

In this paper, a complete measuring pipeline has been implemented, in which all the parameters are under control. This is a big difference with usual software, where the measuring method is usually hidden for the operator. Using simulated scans of a very complex reference part, our aim is to really illustrate the influence of artefacts in the local variation of measurands. Even if the related average errors are not always greatly different due to the high number of measurands, local variations do exist. A visualisation tool allows to help the operator.

Acknowledgements
This study is performed in the frame of the Additive Factory Hub (AFH) platform, located in Ile de France, which aims to finance academic research in the field of metal additive manufacturing.

References

[1] H. Villarraga Gómez, S. Smith, Effect of geometric magnification on dimensional measurements with a metrology-grade x-ray computed tomography system 73 488–503. doi:10.1016/j.precisioneng.2021.10.015.

[2] H. Villarraga Gómez, S. Smith, Effect of the number of projections on dimensional measurements with x-ray computed tomography 66 445–456. doi:10.1016/j.precisioneng.2020.08.006.

[3] P. Hermanek, S. Carmignato, Porosity measurements by x-ray computed tomography: Accuracy evaluation using a calibrated object 49 377–387. doi:10.1016/j.precisioneng.2017.03.007.
URL https://linkinghub.elsevier.com/retrieve/pii/S0141635916304251

[4] Francisco A. Arenhart, Crhistian R. Baldo, Thiago L. Fernandes, Gustavo D. Donatelli, Experimental investigation of the influence factors on the structural resolution for dimensional measurements with CT systems.
URL https://www.ndt.net/search/docs.php3?id=18755&msgID=0&rootID=0

[5] C. Baldo, W. Dewulf, Virtual CT test environment used to study the effect of individual influence factors 9.
URL https://www.ndt.net/search/docs.php3?id=26577&msgID=0&rootID=0

[6] L. A. Feldkamp, L. C. Davis, J. W. Kress, Practical cone-beam algorithm 1 (6) 612–619, publisher: Optical Society of America. doi:10.1364/JOSAA.1.000612.
URL https://www.osapublishing.org/josaa/abstract.cfm?uri=josaa-1-6-612

[7] H. Villarraga-Gómez, E. P. Morse, S. T. Smith, Assessing the effect of penetration length variations on dimensional measurements with x-ray computed tomography 79 146–163. doi:10.1016/j.precisioneng.2022.10.001.
URL https://www.sciencedirect.com/science/article/pii/S0141635922002185

[8] J. Lifton, J. McBride, The application of beam hardening correction for industrial x-ray computed tomography, p. 9.
URL https://www.semanticscholar.org/paper/The-application-of-beam-hardening-correction-for-Lifton-McB
9978ba580f06a7a9841ff26b05062fb5ed05821e

[9] J. J. Lifton, S. Carmignato, Simulating the influence of scatter and beam hardening in dimensional computed tomography 28 (10) 104001, publisher: IOP Publishing. doi:10.1088/1361-6501/aa80b2.
URL https://dx.doi.org/10.1088/1361-6501/aa80b2

[10] ISO, ISO 15530-3:2011.
URL https://www.iso.org/cms/render/live/fr/sites/isoorg/contents/data/standard/05/36/53627.html

[11] P. Müller, J. Hiller, A. Cantatore, L. D. Chiffre, A study on evaluation strategies in dimensional x-ray computed tomography by estimation of measurement uncertainties 3 (2) 107–115, number: 2 Publisher: EDP Sciences. doi:10.1051/ijmqe/2012011.
URL https://www.metrology-journal.org/articles/ijmqe/abs/2012/02/ijmqe120011/ijmqe120011.html

[12] H. Villarraga-Gómez, J. D. Thousand, S. T. Smith, Empirical approaches to uncertainty analysis of x-ray computed tomography measurements: A review with examples 64 249–268. doi:10.1016/j.precisioneng.2020.03.004.
URL https://linkinghub.elsevier.com/retrieve/pii/S0141635919309626

[13] R. Jiménez, M. Torralba, J. Yagüe-Fabra, S. Ontiveros, G. Tosello, Experimental approach for the uncertainty assessment of 3d complex geometry dimensional measurements using computed tomography at the mm and sub-mm scales 17 (5) 1137. doi:10.3390/s17051137.
URL http://www.mdpi.com/1424-8220/17/5/1137

[14] F. Borges de Oliveira, A. Stolfi, M. Bartscher, L. De Chiffre, U. Neuschaefer-Rube, Experimental investigation of surface determination process on multi-material components for dimensional computed tomography 6 93–103. doi:10.1016/j.csndt.2016.04.003.
URL https://www.sciencedirect.com/science/article/pii/S2214657116300089

[15] J. A. Yagüe-Fabra, S. Ontiveros, R. Jiménez, S. Chitchian, G. Tosello, S. Carmignato, A 3d edge detection technique for surface extraction in computed tomography for dimensional metrology applications 62 (1) 531–534. doi:10.1016/j.cirp.2013.03.016.
URL https://www.sciencedirect.com/science/article/pii/S0007850613000176

[16] W. E. Lorensen, H. E. Cline, Marching cubes: A high resolution 3d surface construction algorithm 21 (4) 163–169, number: 4. doi:10.1145/37402.37422.
URL https://doi.org/10.1145/37402.37422